Ligand-Specific c-Fos Expression Emerges from the Spatiotemporal Control of ErbB Network Dynamics

Takashi Nakakuki,[1,7] Marc R. Birtwistle,[2,3,4,7] Yuko Saeki,[1,5] Noriko Yumoto,[1,5] Kaori Ide,[1] Takeshi Nagashima,[1,5] Lutz Brusch,[6] Babatunde A. Ogunnaike,[3] Mariko Okada-Hatakeyama,[1,5,*] and Boris N. Kholodenko[2,4,*]

[1]Computational Systems Biology Research Group, Advanced Computational Sciences Department, RIKEN Advanced Science Institute, 1-7-22 Tsurumi-ku, Yokohama, Kanagawa 230-0045, Japan
[2]Systems Biology Ireland, University College Dublin, Belfield, Dublin 4, Ireland
[3]University of Delaware, Department of Chemical Engineering, 150 Academy Street, Newark, DE 19716, USA
[4]Department of Pathology, Anatomy, and Cell Biology, Thomas Jefferson University, 1020 Locust Street, Philadelphia, PA 19107, USA
[5]Laboratory for Cellular Systems Modeling, RIKEN Research Center for Allergy and Immunology, 1-7-22 Tsurumi-ku, Yokohama, 230-0045, Japan
[6]Dresden University of Technology, Center for Information Services and High Performance Computing, 01062 Dresden, Germany
[7]These authors contributed equally to this work
*Correspondence: marikoh@rcai.riken.jp (M.O.-H.), boris.kholodenko@ucd.ie (B.N.K.)
DOI 10.1016/j.cell.2010.03.054

SUMMARY

Activation of ErbB receptors by epidermal growth factor (EGF) or heregulin (HRG) determines distinct cell-fate decisions, although signals propagate through shared pathways. Using mathematical modeling and experimental approaches, we unravel how HRG and EGF generate distinct, all-or-none responses of the phosphorylated transcription factor c-Fos. In the cytosol, EGF induces transient and HRG induces sustained ERK activation. In the nucleus, however, ERK activity and *c-fos* mRNA expression are transient for both ligands. Knockdown of dual-specificity phosphatases extends HRG-stimulated nuclear ERK activation, but not *c-fos* mRNA expression, implying the existence of a HRG-induced repressor of *c-fos* transcription. Further experiments confirmed that this repressor is mainly induced by HRG, but not EGF, and requires new protein synthesis. We show how a spatially distributed, signaling-transcription cascade robustly discriminates between transient and sustained ERK activities at the c-Fos system level. The proposed control mechanisms are general and operate in different cell types, stimulated by various ligands.

INTRODUCTION

The ErbB receptors initiate a multilayered signal transduction network that converts external cues into specific gene expression responses in different cells and tissues. Its deregulation drives the development and progression of several types of cancer (Citri and Yarden, 2006). Ligand binding causes the homo- and heterodimerization of ErbB receptors, followed by allosteric activation of their intrinsic tyrosine kinases (Zhang et al., 2006). This induces a complex cascade of phosphorylation and activation events that convey signals to the nucleus. The subsequent changes in gene expression eventually lead to pivotal cell-fate decisions, such as proliferation or differentiation.

A major challenge for cell signaling studies is to understand how different cues and receptors give rise to unique gene expression responses despite the promiscuous activation of shared pathways, such as the extracellular regulated kinase 1/2 (ERK) cascade. Initial insight into this specificity dilemma came from observations that PC-12 cells proliferated after a transient ERK activation by epidermal growth factor (EGF) but differentiated after a sustained ERK activation by nerve growth factor (NGF), showing that the duration of ERK signaling is critical for cell-fate decisions (Marshall, 1995). Subsequent theoretical and experimental work revealed that different ERK activation dynamics can arise from differential feedback wiring of the cytosolic ERK cascade (Kholodenko, 2007; Santos et al., 2007). In the nucleus, the duration of ERK activation is sensed by a network of immediate early genes, including the transcription factor c-Fos (Murphy et al., 2004; Murphy et al., 2002). MCF-7 cells show similar signaling input-output relationships: sustained ERK activity induces cellular differentiation and a significant c-Fos response, while transient ERK activity induces proliferation and a negligible c-Fos response (Nagashima et al., 2007). These examples suggest that differential ERK activation kinetics can be converted into all-or-none responses at the transcription factor level. This conversion could explain how common core pathways can program distinct cell-fate decisions.

The sustained induction of c-Fos depends on activation of ERK and its downstream target, p90 ribosomal S6 kinase 2 (RSK), which stimulate *c-fos* transcription and cooperate to stabilize the c-Fos protein product through multiple

phosphorylations (Chen et al., 1992, 1993; Murphy et al., 2002). Phosphorylation also enhances c-Fos transcriptional activity (Pellegrino and Stork, 2006); therefore, phosphorylated c-Fos (pc-Fos) may be viewed as the functional output of this system. A network structure, in which an initial input signal (active ERK) induces an intermediate signal (c-fos messenger RNA [mRNA]) and both the initial and intermediate signals are needed to generate the final output (pc-Fos protein), is termed a coherent feedforward loop (CFL) (Mangan et al., 2003). This CFL creates a "sign-sensitive delay" that senses the duration of ERK activation: a drop in the initial input (− sign) results in immediate loss of output, whereas an increase (+ sign) leads to a delayed increase in output. Additionally, negative feedback regulation arises from ERK-induced expression of the dual specificity phosphatases (collectively known as DUSPs or MAPK phosphatases [MKPs]), which deactivate ERK (Brondello et al., 1997; Brondello et al., 1995; Sun et al., 1993). DUSP protein expression develops on the same time scale as c-Fos expression and is also controlled by ERK activity (Brondello et al., 1999). Thus, although the ERK to pc-Fos CFL could provide a core sensing mechanism for transient versus sustained ERK activity (Murphy et al., 2002), the resulting emergent properties of this network, which includes negative transcriptional regulation are not understood.

Here, we demonstrate how the spatiotemporal coordination of combined signaling and transcriptional responses allows cells to convert analog ERK signaling into robust, digital pc-Fos responses. Although EGF and HRG induce transient versus sustained cytoplasmic ERK activities, downstream c-fos mRNA expression is transient for both ligands. Modeling suggests that this identical c-fos expression duration is explained by a larger dusp expression response and resulting transient nuclear ERK activity for HRG. RNA interference (RNAi)-mediated dusp knockdown sustains HRG-induced nuclear ERK activity but has little effect on HRG-activated c-fos mRNA expression, implying the existence of an additional negative regulator of c-fos transcription. Double-pulse experiments with different ligands demonstrate that this repressor is induced by HRG, but not by EGF. HRG stimulation in the presence of cycloheximide sustains c-fos mRNA expression, showing that activation of the repressor requires de novo protein synthesis. For HRG, sustained cytoplasmic ppERK and, to a lesser extent, the transient nuclear ppERK stabilize the c-Fos protein and drive the high pc-Fos response, whereas for EGF, transient cytoplasmic ERK activity causes a negligible pc-Fos response. Systems-level model analysis reveals how the spatially distributed regulation cascades make the all-or-none pc-Fos responses robust to noise in ERK activity and to system perturbations. Predictions based on our model built for MCF-7 cells can also explain the measured EGF- and NGF-induced pc-Fos responses in the classic PC-12 cell system. Thus, the proposed control mechanisms of discrimination between transient and sustained cytoplasmic ERK activities hold true for different types of cells and ligands. Overall, our experimental and computational results demonstrate that a CFL signaling cascade interlinked with transcriptional negative feedback loops is the principal c-fos regulation module wherein differential, spatially distributed ERK dynamics contribute to binary cell-fate decisions.

RESULTS

Transient and Sustained Cytosolic ERK Activation Signals Are Converted into Similar c-fos Response Durations in the Nucleus

Previous studies showed that activated ERK controls c-fos mRNA expression (Buchwalter et al., 2004; Chai and Tarnawski, 2002). Since EGF and HRG induced transient and sustained ERK activation, respectively (Figure 1A), we expected c-fos mRNA expression to be transient for EGF and sustained for HRG. Surprisingly, c-fos mRNA expression profiles were transient for both ligands, although the magnitude of the c-fos mRNA response was larger for HRG than for EGF (Figure 1B). This difference in the mRNA response was amplified at the level of c-Fos expression (Figure 1C) and converted into an all- (HRG) or-none (EGF) pc-Fos response (Figure 1D). Since ppERK is required for c-Fos stabilization, the observed all-or-none pc-Fos responses can be attributed to the continued ppERK presence after HRG stimulation and the absence of ppERK after 30 min EGF stimulation (Murphy et al., 2002). Yet, this interpretation cannot account for the transient time course of c-fos mRNA. It is also inconsistent with our observations that HRG-induced c-fos mRNA expression begins to decline after 30 min, while ppERK is sustained up to 60 min. These results suggest that the c-Fos expression dynamics cannot be explained solely by the ERK activation profiles and that more complex mechanisms must be invoked.

Building an Initial Computational Model of the c-Fos Expression Network Dynamics

Although some aspects of c-Fos regulation are understood, the data shown in Figure 1 raise several questions. Why are the c-fos mRNA expression profiles transient for both EGF and HRG? What mechanisms are responsible for the all-or-none pc-Fos responses? Is the discrimination mechanism robust to noise and perturbations? To answer such questions, we have developed a mechanistic, computational model that describes the dynamic control of c-Fos expression and phosphorylation (shown schematically in Figure 1E). The model allows us to deeply explore the emergent properties of the signaling network that governs these transitions to make predictions that are used as testable hypotheses in our experiments. When the predictions agree with the data, this substantiates key regulatory mechanisms. On the other hand, points of the model-experiment mismatch call for a new understanding of regulatory mechanisms and model refinement, as indeed happened in this study. Figure 1E shows our initial model (black lines), which is based on pre-existing knowledge. This initial model was used until new experimental data revealed its limitations. The further model refinement (orange lines) incorporates new hypotheses that improve the agreement between the model and experimental data (Figure S1 available online). Here, we briefly describe the initial model; a complete derivation is presented in the Extended Experimental Procedures.

Input Signaling and ERK Dynamics

Understanding of the complexity of signaling can be facilitated by a modular approach to modeling (Kholodenko et al., 2002). This approach allows us to focus only on the ERK-induced c-Fos dynamics, considering signaling between ErbB
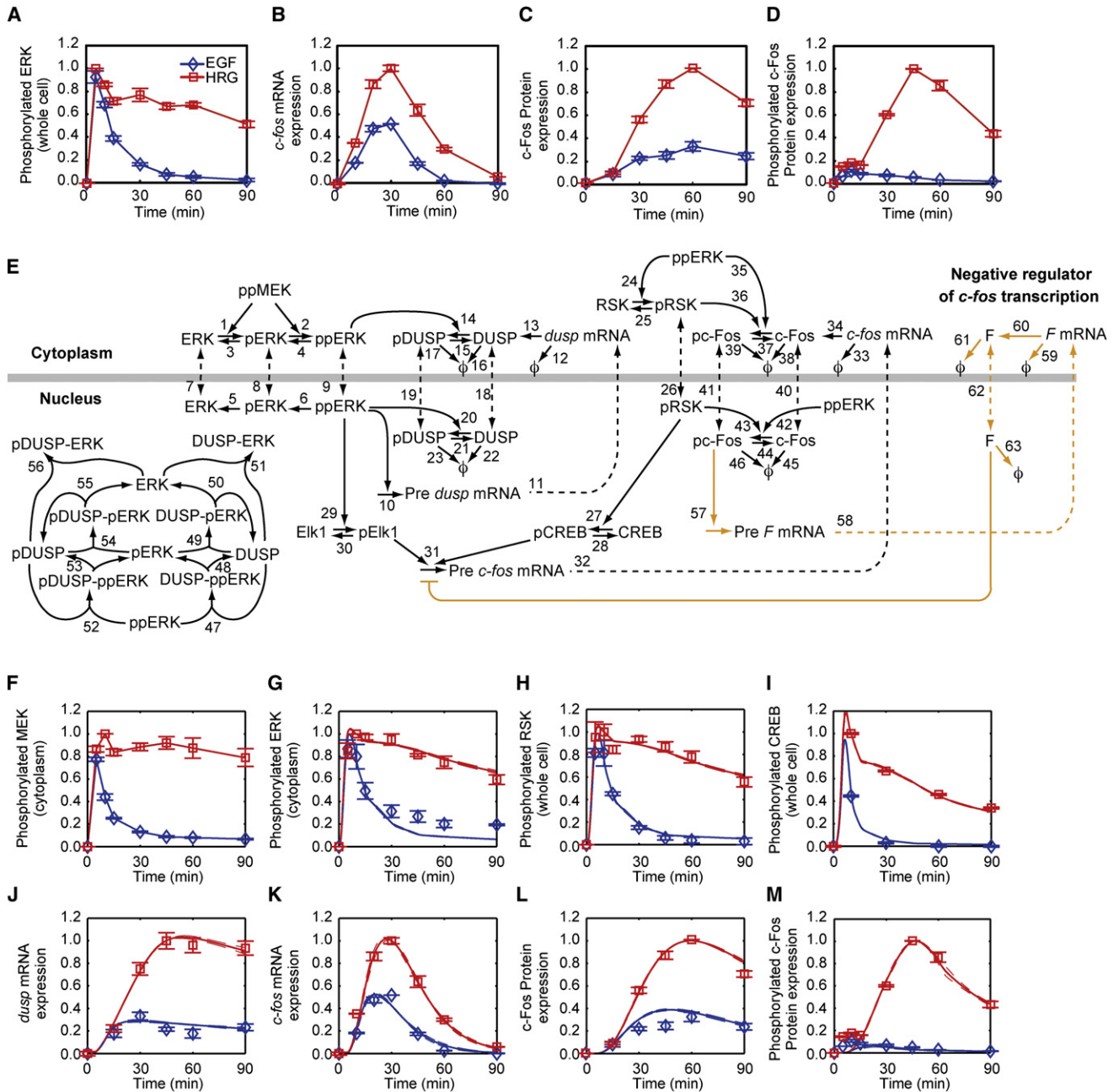
Figure 1. The c-Fos Expression Network: Responses to EGF and HRG and Model's Schematic

MCF-7 cells were stimulated with 10 nM EGF or HRG for indicated periods of time (min), and the responses were measured with western blotting (proteins) or qRT-PCR (mRNA). Data were normalized by dividing them by the maximum value of the HRG-induced responses. Error bars denote standard error for at least three independent experiments; representative blot images can be found in the Figure S1.

(A) ppERK.

(B) *c-fos* mRNA.

(C) Total c-Fos.

(D) T325 phosphorylated c-Fos.

(E) Model's schematic. The nuclear membrane is shown by a thick gray line, chemical transformations are depicted by solid lines, and nucleocytoplasmic transport is denoted by dashed lines. Rate laws and parameters for the individually numbered chemical reactions are given in the Extended Experimental Procedures. Degraded protein and mRNA are represented by φ. Black lines correspond to mechanisms in the initial model, whereas orange lines denote model refinement that is based on additional experimental data (see below).

(F–M) Points (blue diamonds, EGF; red squares, HRG) denote experimental data, solid lines denote simulations done with the initial model, and dashed lines represent these simulations ± standard deviation.

receptors and ERK as a separate module (Birtwistle et al., 2007). As the model input, we take cytoplasmic dually phosphorylated MEK (ppMEK), which activates ERK, and this input is estimated directly from data (Figure 1F). Active ERK is dephosphorylated by constitutive (such as PP2A and PTP-SL) and induced (DUSP) phosphatases in the cytoplasm and nucleus.

c-fos Transcription and Protein Stabilization

Active ERK phosphorylates and activates RSK (Chen et al., 1992), and active ERK and RSK cooperate to stimulate *c-fos* transcription (Figure 1E). Upon nuclear translocation, active ERK phosphorylates and activates the transcription factor Elk1 (Gille et al., 1995), which binds to the serum response factor and subsequently to the *c-fos* promoter (Buchwalter et al., 2004). RSK phosphorylates and activates CREB (Xing et al., 1996), which also binds to the *c-fos* promoter (Wang and Prywes, 2000). When phospho-Elk1 and phospho-CREB are both bound to the *c-fos* promoter, transcription occurs (Bruning et al., 2000; De Cesare et al., 1998). The phosphorylation and stabilization of nascent c-Fos proteins depend on active ERK and RSK and on an ERK docking site on c-Fos termed the DEF domain (Murphy et al., 2002).

dusp Transcription and Protein Stabilization

The nuclear inducible *dusps* are immediate early genes that are upregulated within ~15–30 min of stimulation with EGF in a variety of cell lines (Charles et al., 1992; Keyse and Emslie, 1992). ERK activation leads to upregulation of *dusp* mRNA levels (Brondello et al., 1997), and, similar to c-Fos, active ERK phosphorylates and stabilizes the *dusp* protein product (Brondello et al., 1999). DUSP translocates to the nucleus and dephosphorylates nuclear ppERK (Brondello et al., 1995).

Training the Model with Experimental Data

Before a model can be used to generate hypotheses, it must be "trained" with experimental data. This process is called parameter estimation (see details in the Experimental Procedures and Extended Experimental Procedures). To train the model, we used data on multiple nodes of the c-Fos expression network (Figures 1F–1M). The solid lines in Figures 1F–1M denote simulations done with the initial model that match closely with the data (shown as points). Although the model can reproduce the data in Figure 1, goodness of fit to a training set alone is insufficient for validating the model. It is necessary to test the model predictions against independent experimental data, as is described below.

Sensitivity Analysis Suggests Critical Control Mechanisms of c-Fos Induction

The model permitted us to analyze on a systems level how transient (EGF) and sustained (HRG) ERK signals are robustly discriminated into all-or-none pc-Fos responses, despite the same duration of *c-fos* mRNA responses. To generate testable hypotheses, we employed sensitivity analysis, which examines how perturbations to the processes in the model affect the *c-fos* mRNA expression duration and cumulative (time-integrated) pc-Fos protein response. We quantified the duration as the time it takes for *c-fos* mRNA to decline below 10% of its maximum and the cumulative response as the integral of the pc-Fos concentration over the observation time of 90 min. The sensitivities, or control coefficients, were approximated as the percent change in the quantity of interest caused by a 1% change in a reaction rate (Kholodenko et al., 1997b). Negative control coefficients indicate that the quantity will decrease with a reaction rate increase, while positive coefficients indicate that the quantity will increase. Large coefficients, whether positive or negative, indicate potentially significant control mechanisms.

The control coefficients for *c-fos* mRNA duration and integrated pc-Fos response are presented in Figures 2A and 2B (see also Figure S2). For both EGF and HRG, the dynamic expression of *c-fos* mRNA is strongly controlled by *c-fos* transcriptional processes (including mRNA transport and degradation). EGF and HRG differ in *dusp* mRNA production/degradation, ERK (de)activation and transport, and the RSK-CREB pathway contributions. The control distribution over the cumulative pc-Fos response (Figure 2B) also shows that *dusp* expression contributes to the ligand-specific regulation of pc-Fos. While sensitivity analysis suggests an appreciable regulatory role of *dusp*, this analysis considers only small perturbations, and the predictions may not hold for large perturbations. Therefore, we evaluated how large decreases in *dusp* mRNA levels would affect *c-fos* responses. The results support the conclusions of the sensitivity analysis. Simulated *dusp* downregulation increased the amplitude and duration of *c-fos* mRNA responses for HRG, but only the amplitude for EGF (Figures 2C and 2D).

Pivotal Role of Negative Feedback Regulations in Ligand-Dependent c-Fos Responses and Construction of a Refined Model
Nuclear ERK Signaling Is Transient for Both HRG and EGF

Our model predicts that although HRG induces sustained *cytoplasmic* ERK activity (Figure 1G), HRG-induced *dusp* expression results in transient *nuclear* ERK activation, which persists slightly longer for HRG than for EGF (Figure 3A). To test this prediction, we quantified the spatially-resolved dynamics of ppERK by
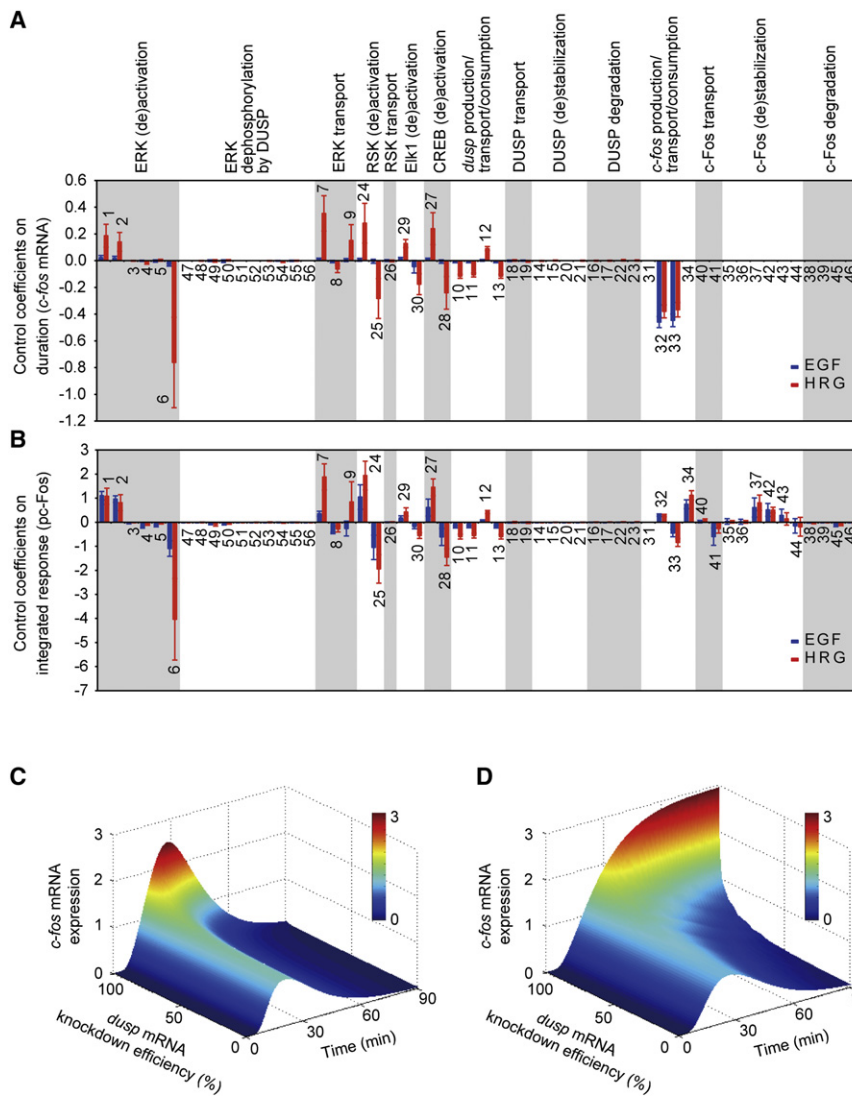

(F) Cytoplasmic MEK activation.
(G) Cytoplasmic ERK activation.
(H) Whole-cell RSK phosphorylation.
(I) Whole-cell CREB phosphorylation.
(J) *dusp* mRNA expression.
(K) *c-fos* mRNA expression.
(L) Whole-cell c-Fos expression.
(M) Whole-cell c-Fos phosphorylation.
See also Figure S1 and Tables S1, S2, S3, and S4.

Figure 2. Sensitivities of *c-fos* mRNA Duration and Integrated pc-Fos Responses to Perturbations

Simulations are done with the initial model; ligand concentrations are 10 nM. For the calculated sensitivity coefficients to obey summation laws, a time-invariant model input is needed, but the input for the initial model (Figure 1F) varies with time. We therefore use the empirical input model described in Figure S2, which has a constant input, to perform the sensitivity analysis.

(A and B) Control coefficients for *c-fos* mRNA duration (A) and integrated pc-Fos (B) are shown by bars (blue, EGF; red, HRG). Numbers above bars indicate the reaction indices as shown in Figure 1E, and error bars correspond to simulation standard deviation. Reactions are grouped according to biological processes (indicated above each plot) and not in the order of their numerical index.

(C and D) Simulated effects of various degrees of *dusp* knockdown on EGF-induced (C) and HRG-induced (D) *c-fos* mRNA expression. Downregulation of *dusp* is simulated by increasing the *dusp* mRNA degradation rate constant.

See also Figure S2.

immunofluorescence staining (Figures 3B–3D and Figure S3A). The data confirmed that both the HRG and EGF-induced nuclear ppERK profiles are transient. During the time interval between 15 min (after both ligands have evoked similar peak responses) and 60 min (when responses return to basal levels), the time-averaged nuclear ppERK concentration is about 1.5-fold larger for HRG than for EGF (represented by the shaded areas in Figures 3B and 3C). The difference between the EGF and HRG responses during this time window is highly significant (a one-tailed, two-sample t test gives $p = 0.0084$). Notably, this difference is similar to the difference between the peak magnitudes of the downstream HRG- and EGF-induced *c-fos* and *dusp* mRNA expressions (Figures 1J and 1K). Thus, the time-averaged nuclear ppERK activity is a biochemical indicator of downstream immediate early mRNA responses.

Effects of dusp Knockdown on the c-fos mRNA, Nuclear ppERK, and pc-Fos Protein Responses

The model predicts that *dusp* downregulation increases both the duration and magnitude of *c-fos* mRNA expression for HRG,

while increasing only the response magnitude for EGF (Figures 2C and 2D). To test this experimentally, we downregulated the major nuclear inducible *dusps* by small interfering RNA (siRNA). In MCF-7 cells, *dusps 1, 2, 4, 5, 8,* and *10* are induced, but expression levels of *dusps 8* and *10* for HRG are relatively small compared to those of *dusps 1, 2, 4,* and *5* (Figure S3B). Moreover, recent studies indicated that only the joint inhibition of *dusps 1, 2, 4,* and *5* markedly influenced nuclear ERK2 activation (Armstrong et al., 2009; Caunt et al., 2008). Therefore, we measured EGF and HRG-evoked *c-fos* mRNA responses after the simultaneous knockdown of *dusps 1, 2, 4,* and *5*. For EGF, the data agree with the model prediction (Figure 3E). However, for HRG, *dusp* knockdown only slightly increased the magnitude of the *c-fos* mRNA response. In contrast to our model predictions, there was little effect on the response duration (Figure 3F), despite the fact that nuclear ppERK was enhanced, as expected (Figures S3E and S3F). Nevertheless, *dusp* knockdown slightly increased HRG-induced c-Fos and pc-Fos levels (Figures S3E and S3F), reflecting the increased nuclear ppERK level, which caused increased phosphorylation and faster stabilization of c-Fos.

Ligand-Dependent Negative Feedback Regulation of c-fos Expression

The *dusp* knockdown experiments showed that for HRG, the *c-fos* mRNA responses remained transient, while nuclear ppERK became sustained, suggesting that HRG, but not EGF, induces a repressor of *c-fos* transcription. If this repressor is
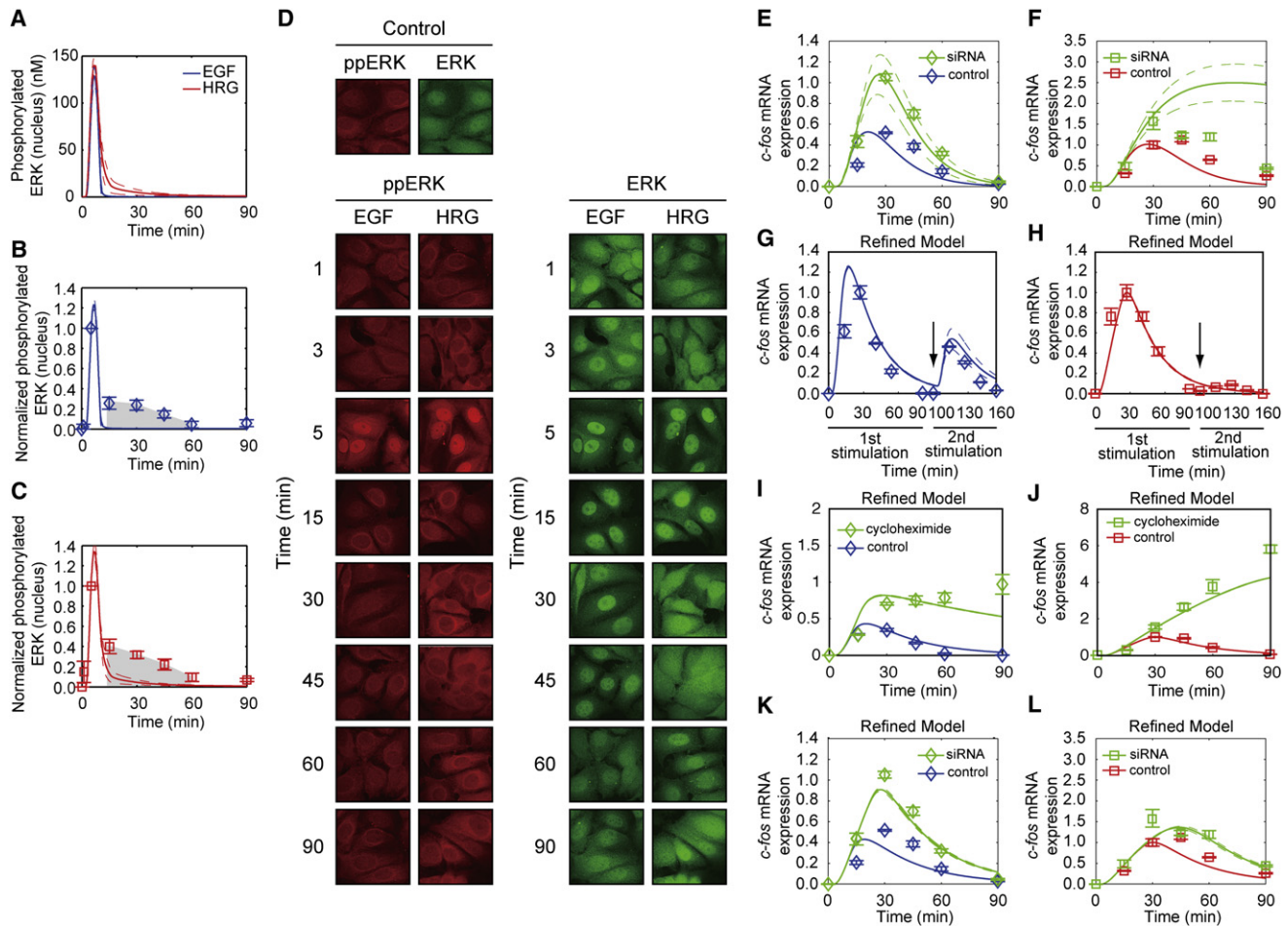
Figure 3. Nuclear ERK Activation Dynamics and the Effect of *dusp* Downregulation on *c-fos* mRNA Duration

(A) Model predictions for nuclear ppERK time courses. Ligand concentrations are 10 nM (EGF, blue; HRG, red).

(B and C) Quantified nuclear ppERK dynamics based on cell images obtained from Duolink technology (EGF, blue; HRG, red; representative images are shown in Figure S3A). Each data point is the average response based on ~180 individual cells in three independent experiments, and error bars correspond to standard error based on the three replicates. Solid lines denote in silico simulations, and dashed lines denote simulation standard deviation. For normalization, raw quantified data are divided by the 5 min time point of each respective ligand dose. Shading corresponds to the nuclear ppERK profile between 15 and 60 min.

(D) Spatially resolved ERK activation dynamics observed by immunofluorescence. Total ERK (green) is shown on the right, and ppERK (red) is shown on the left.

(E, F, K, and L) Measured versus predicted effects of *dusp* downregulation on *c-fos* mRNA expression induced by 10 nM EGF (E and K) or HRG (F and L). Solid and dashed lines correspond to model simulations and their standard deviation, respectively. The *dusp* downregulation was modeled as an increase in the *dusp* mRNA degradation rate. Simulations in (E) and (F) correspond to the initial model (Figure 1E, black lines only), and simulations in (K) and (L) correspond to the refined model (Figure 1E, black and orange lines).

(G and H) *c-fos* mRNA expression in response to two 1 nM pulses of EGF (G) or HRG (H). Arrows denote the second stimulation time.

(I and J) Effects of cycloheximide on *c-fos* mRNA expression induced by 10 nM EGF (I) or 10 nM HRG (J).

For (E)–(L), error bars denote the standard error from three independent experiments. Note that (I) and (J) have different y axis scales. In (E), (F), and (I)–(L), data values are relative to their respective 30 min HRG control point. Solid and dashed lines correspond to model simulations and their standard deviation, respectively. Simulations done with the refined model are indicated.

See also Figure S3.

transcriptionally activated, it would probably persist beyond 90 min after stimulation, when *c-fos* mRNA decreases to basal levels. Then, a second pulse of HRG added 90 min after the initial HRG stimulation would be unable to induce significant *c-fos* mRNA expression, whereas a second EGF pulse would still evoke a large *c-fos* mRNA response after initial EGF stimulation. Figures 3G and 3H (diamonds for EGF, squares for HRG) demonstrate that a second HRG-pulse indeed caused a negligible *c-fos*

mRNA response, whereas a second EGF-pulse stimulated a significant response (while ERK is activated in either case; see Figure S3G). This negative feedback regulator hypothesis is further supported by additional double-pulse experiments in which various ligands are added in different orders. A pulse of HRG added 90 min after EGF induced a significant *c-fos* mRNA response, whereas a pulse of EGF added 90 min after HRG did not (Figure S3G). We also replaced HRG with PMA,

a phorbol ester that induces sustained ERK activation similarly to HRG (see below). An EGF pulse after PMA stimulation generated a negligible *c-fos* mRNA response. On the other hand, a PMA pulse given after EGF induced a strong *c-fos* mRNA response (Figure S3G).

Since the timing of this HRG-induced feedback suggests that it may require de novo protein synthesis, we measured the HRG and EGF-induced *c-fos* mRNA responses in the presence of the protein synthesis inhibitor cycloheximide (CHX). CHX markedly increased the HRG-induced *c-fos* mRNA but had a smaller effect on the EGF-induced response (Figures 3I and 3J). The change from the transient HRG-induced *c-fos* mRNA response to the sustained response in the presence of CHX can partly be explained by CHX-induced increases in the *c-fos* mRNA half-life (Sariban et al., 1988). Yet, this extension of half-life alone cannot account for the CHX effect; a simple mathematical model demonstrates that a concomitant change that sustains the *c-fos* transcription rate is needed (Extended Experimental Procedures and Figure S3H). Analysis of a previously published gene chip data set identified 40 transcriptional regulators that are upregulated upon HRG stimulation, and are thus candidates for this negative regulatory factor (Table S5) (Nagashima et al., 2007).

A Refined Model of c-fos Regulation
The data obtained from *dusp* knockdown, double-pulse and CHX experiments cannot be explained by our initial model of *c-fos* regulation (black lines in Figure 1E). Therefore, we refined this model to include an additional layer of negative transcriptional control. A scenario consistent with this negative regulator hypothesis is that pc-Fos induces its own transcriptional repressor, as shown schematically by the orange lines in Figure 1E, or directly inhibits *c-fos* transcription. In fact, it was previously reported that the c-Fos protein can repress its own promoter (Schönthal et al., 1988; Superti-Furga et al., 1991). Upon training our refined model to the data, we found that it not only reproduced the original training data set, but also reproduced the nuclear ppERK dynamics better than the initial model (Figure S1B). The simulations capture that the HRG-induced nuclear ppERK profile is higher than the EGF-induced profile during the 15–60 min time frame, in line with the experimental findings (see the shaded areas in Figures 3B and 3C). Using the refined model, we computed the effects of *dusp* downregulation on the EGF- and HRG-induced *c-fos* mRNA kinetics (Figures 3K and 3L) and found a reasonable agreement between the data and simulations. Importantly, this refined model predicts the results of double-pulse experiments (Figures 3G and 3H and Figure S3G) and accounts for the CHX experiments (Figures 3I and 3J), which the initial model fails to predict.

We conclude that transcriptional negative feedback, which includes *dusps* and a yet unknown *c-fos* repressor(s), plays a larger role in regulating the duration of HRG-induced than EGF-induced *c-fos* mRNA expression. Although the refined mechanistic model can describe the system dynamics, the identity of the negative regulator is as yet unknown. When mechanistic details become available, our model will be further improved to incorporate a complete description of processes that activate this repressor.

General Operating Principles and Ubiquitous Control Mechanisms of c-Fos Expression
A Core Model Description of the Emergent Properties of the c-Fos System
Motivated by the quest to understand the key regulatory principles of the c-Fos expression system, we developed a "core" model, which compared to the mechanistic model is deliberately simplified to capture the essential system characteristics. Our core model takes cytoplasmic ppERK as input, involves only five intermediates, and has pc-Fos as the output (Figure 4A; for details see the Extended Experimental Procedures). In the core model, nuclear pRSK and ppERK together stimulate transcription of *c-fos*, and cytoplasmic ppERK phosphorylates the c-Fos protein. We represent the overall transcriptional negative feedback as dependent on the cumulative (i.e., integrated over time) nuclear ppERK activity, assuming that the current levels of these negative regulators reflect the recent history of the nuclear ppERK profile. This single negative feedback implicitly accounts for both DUSPs and the unknown transcriptional repressor, since the cumulative nuclear ppERK activity is representative of growth factor-induced transcriptional responses. In fact, nearly perfect adaptation of *c-fos* mRNA responses in which the response returns to the basal level supports this assumption. In engineering terms, this feedback is called "integral feedback," which endows most control systems with perfect adaptation capabilities (Mettetal et al., 2008; Ogunnaike and Ray, 1994).

The core model was trained using only a single ligand dose (10 nM EGF and 10 nM HRG) to describe the measured *c-fos* mRNA and pc-Fos protein responses in MCF-7 cells (Figures 4B–4D and Figure S4). To test this model, we compared its predictions to measured pc-Fos responses for *different* EGF and HRG doses (Figures 4E–4H). The agreement between model predictions and the experimental data substantiates our core model.

Robustness of the c-Fos Expression System
The core model encapsulates the key features of the c-Fos system (Figure 4A): (1) an outer CFL (cytoplasmic ppERK and c-Fos generate pc-Fos), (2) an inner CFL (nuclear ppERK and pRSK activate *c-fos* transcription), and (3) an integral transcriptional negative feedback. The importance of the outer CFL for converting transient versus sustained ppERK signals into all-or-none c-Fos responses was previously shown (Murphy et al., 2002). However, the systems-level roles of the inner RSK-mediated CFL and the transcriptional negative feedback remain unclear.

This structure of the c-Fos system, where an inner CFL is embedded into an outer CFL, resembles a cascade organization of feedback controllers in engineering control systems that provides robustness of the output to disturbances in the input (Ogunnaike and Ray, 1994). Therefore, we simulated how disturbances to the ppERK input signal, in the form of a sine wave, affect the integrated pc-Fos response in the presence or absence of the inner CFL. In response to the same level of ppERK disturbance, the system with the inner CFL produced a much lower cumulative pc-Fos output than the system without the inner CFL (Figures 5A and 5B). Only disturbances that persist as long as HRG-induced ppERK activation cause appreciable
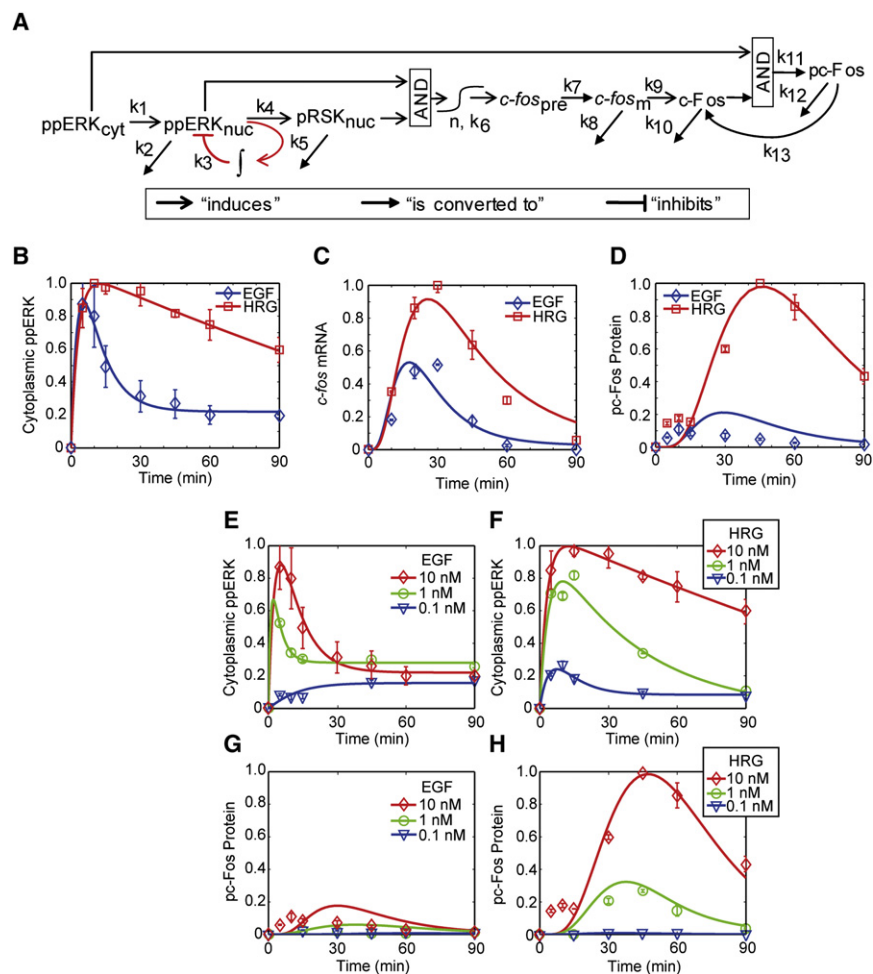
Figure 4. Core c-Fos Expression Model
(A) Model schematic.
(B–D) The core model parameters were trained by the responses of ppERK, *c-fos* mRNA, and pc-Fos to 10 nM EGF or 10 nM HRG in MCF-7 cells.
(E–H) To validate the model, we compared model predictions to the observed pc-Fos responses for different EGF and HRG doses (1 nM and 0.1 nM) in MCF-7 cells. Experimental data were obtained with western blotting (proteins) or qRT-PCR (mRNA).
Error bars denote standard error for at least three independent experiments, and representative western blot images can be found in Figure S4. For all time course plots, solid lines denote simulations.
See also Figure S4.

from MCF-7 cells (Figures 6A–6E). In our simulations, only the ppERK input profile was allowed to vary with respect to MCF-7 cells; *all other parameter values remained fixed.* When the input for our MCF-7 cell model corresponded to PC-12 cell ERK signaling, the calculated c-Fos dynamics qualitatively agreed with the measured c-Fos expression and activation responses in PC-12 cells (Figures 6B and 6C). The major difference was that the predicted *c-fos* mRNA expression dynamics were slower than observed, perhaps because MCF-7 and PC-12 cells originated from different human and rat cells, respectively, which may have different *c-fos* mRNA half-lives.

Comparison of Figure 6A to Figure 1A shows that EGF induces a slightly more sustained ppERK signal in PC-12 cells than in MCF-7 cells. Yet despite this longer ppERK signal duration, the pc-Fos response remains small for EGF (Figure 6C), demonstrating the robustness of the system to discriminate transient versus sustained ppERK signals. Overall, these results suggest that the control mechanisms of c-Fos expression responses built into our model are general, rather than limited to MCF-7 cells.

PMA-Enhanced, EGF-Induced ERK Activation Amplifies the c-Fos Expression Response

Are the ERK activation kinetics a master regulator of the ligand-dependent, all-or-none pc-Fos response? To address this question, we costimulated MCF-7 cells with EGF and PMA, a potent activator of PKC that extends EGF-induced ppERK dynamics to a profile similar to that of HRG (Figure 6D). Thus, if the pc-Fos response solely depended on the ERK activation kinetics, rather than the nature of the ligand or upstream receptor, we would expect that EGF and PMA costimulation results in a large pc-Fos response, similar to the HRG-induced response. This is exactly what the core model predicts, and what was observed experimentally (Figure 6E). These results support the emerging paradigm that ligand specificity is related to the different spatio-temporal dynamics of shared, core signaling outputs, which
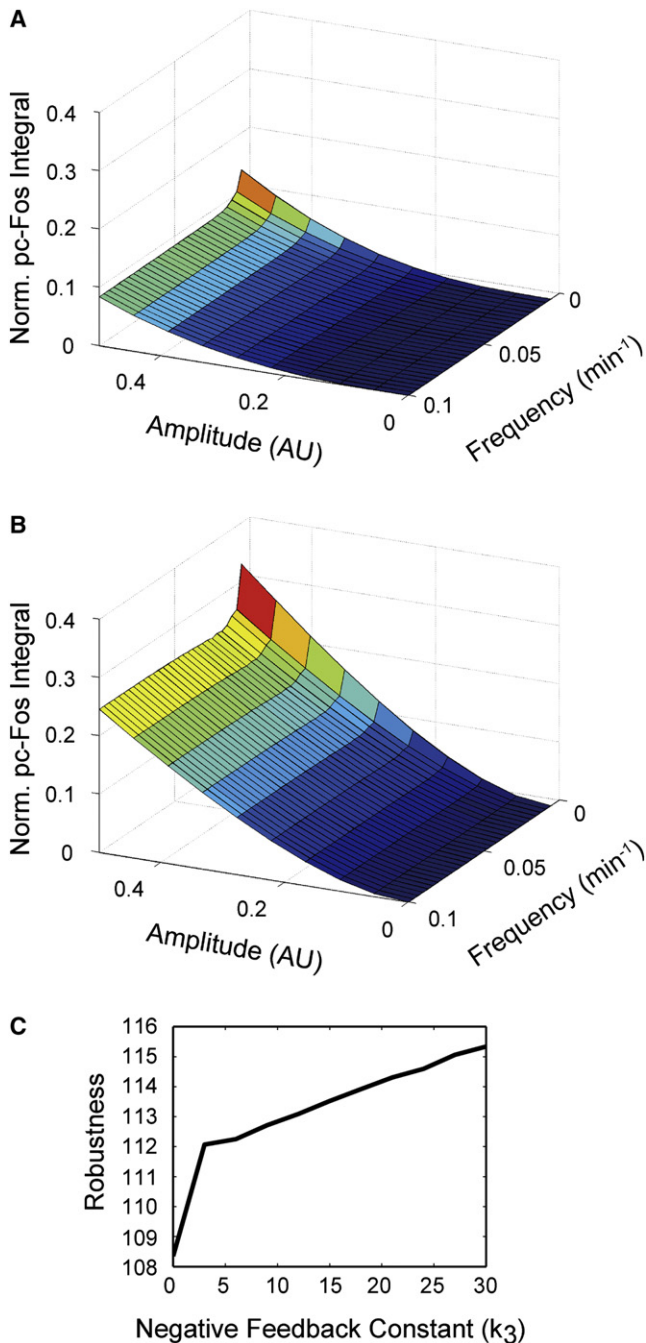
pc-Fos output. These results suggest that the inner CFL makes the integrated pc-Fos output robust to noisy ppERK signals.

The transcriptional negative feedback loops not only make the c-Fos response transient, but can also endow the system with robustness (Sauro and Kholodenko, 2004). We therefore investigated how sensitive the integrated pc-Fos output was to perturbations in the system parameters at different negative feedback strengths (see the Experimental Procedures). Indeed, as the negative feedback strength is increased, the cumulative pc-Fos response becomes more robust (Figure 5C). Thus, the transcriptional negative feedback, in addition to shaping the dynamics of the pc-Fos response, provides robustness to system parameter perturbations.

EGF- versus NGF-Induced pc-Fos Responses in PC-12 Cells

Are key control features of the c-Fos expression system specific to MCF-7 cells, or are they applicable to other cells? To answer this question, we revisited the classic PC-12 cell system wherein transient or sustained ppERK signals lead to distinct cell-fate decisions (Marshall, 1995). We measured the dynamics of ppERK, *c-fos* mRNA, and pc-Fos in PC-12 cells stimulated with 10 nM EGF or 10 nM NGF and compared these data to the predictions of our core model that was trained by data

Figure 5. Robustness of the c-Fos Expression Network

(A and B) Robustness to disturbances in ppERK increases when the inner CFL is present (A) and decreases when this CFL is absent (B). Disturbances are simulated as $|A\sin(\omega t)|$, where A is the amplitude, ω is the frequency, and t is time. AU stands for arbitrary units. These arbitrary units correspond to the same arbitrary units characterizing cytoplasmic ppERK measurements in Figures 1G, 4B, and 4E. The inner CFL is "absent" when the dependence of *c-fos* transcription on pRSK is disregarded in the model. The integrated pc-Fos response is expressed in the units relative to the 10 nM HRG response. (C) Robustness of the c-Fos expression system increases with increasing the integral negative feedback strength (k_3). Robustness is quantified as the sum over all inverse, absolute control coefficients of system parameters (the

consequently induce differential gene expression responses. Both our core and refined mechanistic models substantiate this paradigm by clear-cut computational findings.

Precise Relation between the ppERK Kinetics and pc-Fos Response

Having shown that differential ERK activation dynamics can qualitatively determine the c-Fos response, we asked which exact quantitative features of the dynamic profiles of cytoplasmic ppERK are responsible for this decision. To this end, we first approximated the ppERK dynamics with three quantitative parameters, the peak amplitude, A_p, the time to peak, T_p, and the decay time, τ (Figure 6F). We then created a family of different ppERK inputs by combinatorially varying these parameters, and finally, calculated the cumulative pc-Fos output for each of these different inputs (see Figure S5 for the full results). Experimentally, we complemented the simulations by measuring ppERK dynamics induced by various concentrations of EGF and HRG in MCF-7 cells and EGF and NGF in PC-12 cells, respectively. Given typical A_p and T_p values for ERK activation dynamics, the mathematical model suggests a simple result, which is supported by the experimental data: the cumulative pc-Fos response is determined by the decay time of ppERK in both cell lines (Figure 6G). Importantly, this emergent relationship serves to convert the previous, qualitative ERK signaling paradigm into a precise, quantitative understanding of how the ppERK dynamics control the all-or-none pc-Fos responses.

DISCUSSION

Cell signaling research is challenged with the question of how ligand specificity can emerge when different pathways share the same core components (Kholodenko, 2006). In the current study, we combined computational modeling and experiments to provide insight into this question. The models bring together extensive previous experimental data with our own new data to unveil that ligand-specific pc-Fos responses are brought about by a spatially distributed control system that involves a cascade of CFLs interlinked with transcriptional negative feedback loops. Owing to the time lag between transcription initiation and translation, this cytoplasmic-signal-to-protein-expression CFL structure acts as an "AND gate" to convert the sustained versus transient *cytoplasmic* ppERK temporal profiles into the all-or-none pc-Fos responses. Negative transcriptional feedback not only causes the similar *c-fos* expression durations for EGF and HRG, but also endows the pc-Fos response with robustness to parameter perturbations. The "inner" CFL involving RSK makes pc-Fos robust to noise in the ppERK input.

In this work, we developed a mechanistic model and a core model, which serve complementary purposes. The mechanistic model allows us to ascribe observed behavior to precise biochemical mechanisms, aiming to create an in silico replica of cellular networks. Mechanistic biochemical models are directly tested against experiments, but these models must be refined continuously to keep pace with the constantly increasing

greater this sum is the smaller the changes that occur when parameters are perturbed; see the Experimental Procedures).
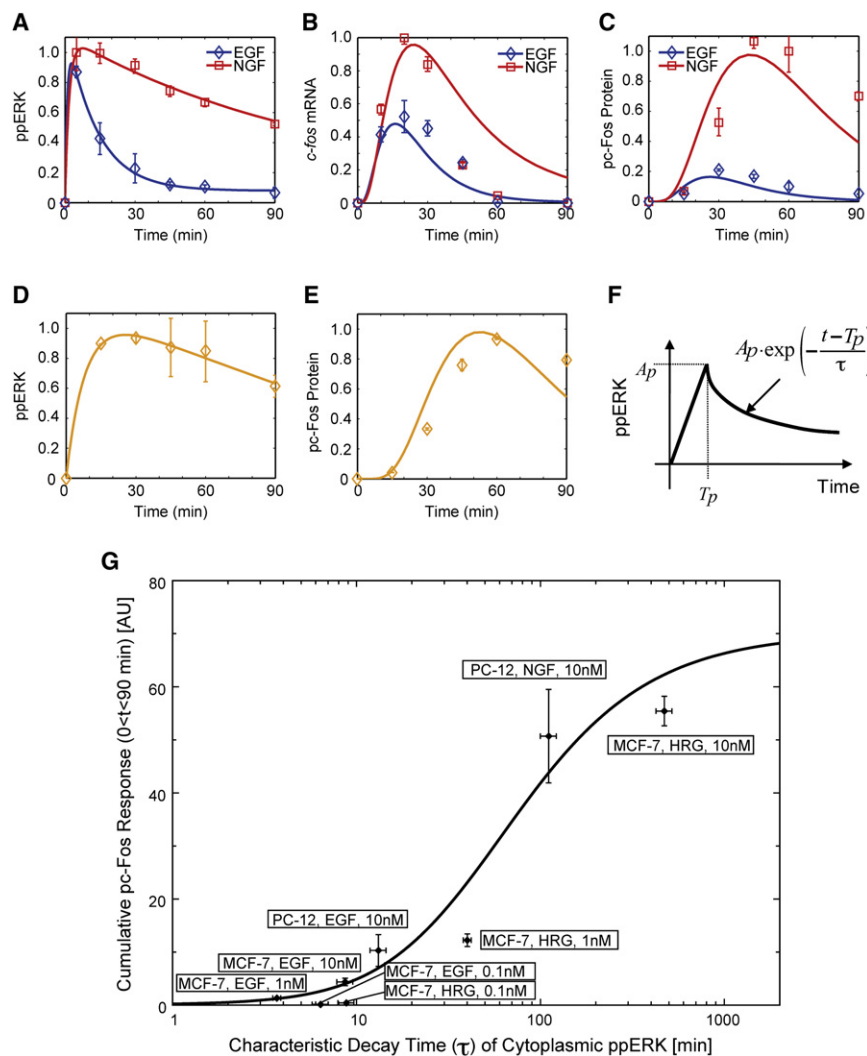
Figure 6. ERK activation Is a Ubiquitous Master Regulator of the Integrated pc-Fos Responses

(A–C) PC-12 cells were stimulated with 10 nM EGF or 10 nM NGF for indicated periods of time, and responses were measured with western blotting (proteins) or qRT-PCR (mRNA). Data were normalized by dividing them by the maximum value of the HRG-induced responses.

(D and E) MCF-7 cells were stimulated with 10 nM EGF + 100 nM PMA.

(F) The ppERK input is characterized by three parameters: the peak amplitude A_p, the peak time T_p, and the decay time τ.

(G) Quantitative relationship between the integrated pc-Fos output and the ppERK decay time τ. Data points correspond to experimental data for various ligand doses in MCF-7 and PC-12 cells, which are indicated by text boxes. The ppERK decay time τ was calculated from experimental data (see the Extended Experimental Procedures, Core Model Description, τ_{in}^d). For simulations, the values for A_p and T_p were fixed at 1 and 10 min., respectively, as is commonly observed for ppERK responses. Calculation of the integrated pc-Fos responses from experimental data is described in the Extended Experimental Procedures.

For all relevant panels, error bars denote standard error for at least three independent experiments, representative blot images can be found in Figure S5, and solid lines denote simulations. For all panels, simulations were done using the core model.

See also Figure S5.

detailed knowledge of molecular mechanisms. The current study, in which we refined our initial model following the results of siRNA, double-ligand pulse, and CHX experiments, exemplifies this continuous refinement. Nevertheless, mechanistic models have large potential to facilitate understanding complex signaling networks. However, when the detailed mechanistic knowledge is lacking, it is desirable to employ simple, core models. Core models do not have excessive numbers of species and parameters but capture and explain the key features that control the system behavior. Our core model serves just this purpose; when our data showed the limitations of the current knowledge, the core model helped us comprehend the emergent properties of the c-Fos expression network.

The biological significance of the CFL-regulated pc-Fos response is that a robust switch-like activation of transcription factors will lead to drastically different subsequent waves of gene expression, and consequently different phenotypes. The CFL structure also allows the cell to turn off gene expression rapidly as soon as the input signal is lost, while buffering the cell against unwarranted gene expression in response to

spurious inputs or noise (Figure 7A). In addition to these cytoplasmic-signal-to-protein-expression CFLs, active nuclear ERK, RSK, and c-fos mRNA generate the nuclear-signal-to-mRNA CFL that operates on a shorter time scale (Figure 7B). These fast and slow CFLs are organized in a "cascade" structure, where the faster, "inner" loop (ppERK-pRSK-c-fos mRNA) operates within the context of the slower, "outer" loop (ppERK-c-fos mRNA-pc-Fos protein). Because it takes time to propagate the disturbances in cytoplasmic ppERK through the inner loop before they reach c-fos mRNA, the inner loop filters fast ppERK input noise. When this cascade CFL structure is combined with the transcriptional negative feedback loops, which make the system robust to parameter perturbation, the overall network acquires even greater noise reduction capabilities (Figure 7C).

Why does the cell employ *dusp* and additional *c-fos* repressor(s) to downregulate the *c-fos* mRNA response when in principle the *dusp* response alone should be adequate for this task? One reason is that functional redundancy leads to robustness against system failures resulting from breakdown of any single component. This is a universally desirable feature that conceivably may have been selected for during evolution. Another, less obvious reason arises from the double-ligand pulse experiments, which show that an unidentified *fos* repressor
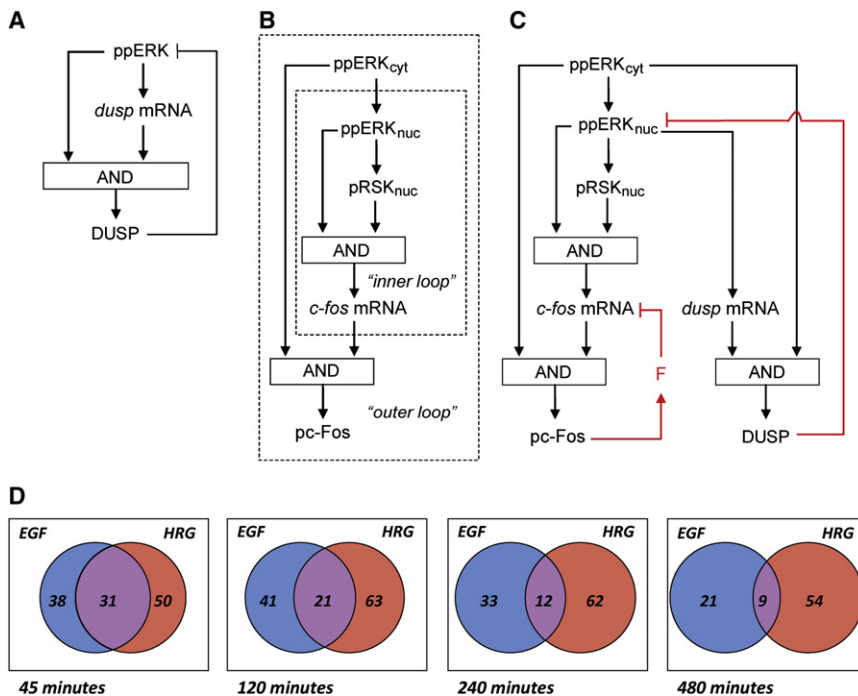
Figure 7. Regulatory Motifs in the c-Fos Expression Network and Emerging Differential, Long-Term Transcription Factor Expression

(A) DUSP negative feedback superimposed onto the CFL.

(B) The CFL cascade structure of c-Fos regulation wherein the fast, nuclear inner CFL is contained within the slow, cytoplasmic outer CFL.

(C) The overall network structure which includes the cascade CFL embedded into the transcriptional negative feedback loops.

(D) Venn diagrams showing the number of common differentially expressed TFs between the EGF and HRG responses. The EGF (left, blue) and HRG (right, red) sets correspond to the number of differentially expressed gene probes that were identified as transcription factors by query to the gene ontology database.

See also Figure S6.

makes MCF-7 cells refractory to further ligand stimulation in terms of *c-fos* expression. Thus, expression of this additional repressor converts cells into a different state, in which they no longer respond to ligands. Since HRG stimulation causes MCF-7 cell differentiation, the *c-fos* repressor may play a key role in ensuring that the cells follow the differentiation pathway despite the potential presence of other signals.

The opposing cell-fate decisions caused by EGF and HRG (proliferation versus differentiation) should be underlined by distinct gene expression patterns. We suggest that the *quantitative* differences in *c-fos* mRNA expression at the immediate early gene level are translated into robust *qualitative* differences for later waves of gene expression changes. Differences in expression of immediate early transcription factors such as *c-fos* would have a large impact on successive gene expression waves, if these factors are hubs in the regulatory network. As network hubs have many interaction partners and the DEF domain is critical for the all-or-none pc-Fos response (Murphy et al., 2002), we looked at the number of interaction partners for transcription factors with and without DEF domains. We indeed found that transcription factors with a DEF domain had a larger mean number of interaction partners (23.1) than non-DEF domain containing factors (15). For DEF domain-containing transcription factors known to be HRG-induced immediate early responders in MCF-7 cells, the mean number of interaction partners (44) was even larger (Figure S6) (Nagashima et al., 2007). Our hypothesis is further supported by previously published gene expression responses to HRG and EGF over longer time periods (Figure 7D) (Nagashima et al., 2007). At early times (45 min), nearly all the transcription factors that are differentially expressed in response to EGF and HRG are shared. However, as time progresses the overlap between these two sets decreases dramatically. We hypothesize that in large part this is due to

HRG-induced, pc-Fos protein controlled gene expression. We propose that this quantitative-to-qualitative gene expression control principle may be general to mammalian signal transduction systems that induce distinct cell fates. Thus, we suggest that the integral negative feedback-embedded, cascade CFL structure that controls the initial, robust switch-like pc-Fos response is critical for control of cell-fate decision processes.

EXPERIMENTAL PROCEDURES

Cell Culture and Treatment

MCF-7 cells were maintained and stimulated as previously described (Birtwistle et al., 2007). PC-12 cells were purchased from RIKEN Bioresource Center (Tsukuba, Japan) and maintained in Dulbecco's modified Eagle's medium (DMEM) supplemented with 10% horse serum and 10% fetal bovine serum (FBS). NGF was purchased from R&D Systems, (Minneapolis, MN). Where indicated, serum starved cells were pretreated with cycloheximide (CHX) (Nacalai Tesque, Japan) or simultaneously treated with the PKC activator, Phorbol 12-Myristate 13-Acetate (PMA) (Nacalai Tesque). For double-pulse experiments, cells were treated with 1 nM EGF or HRG and incubated for 90 min, washed three times with serum-free medium over 10 min., and then treated again with the same concentration of each growth factor. For different ligand combinations, 30 nM was used for EGF and HRG to induce full receptor activation, such that ErbB receptor crosstalk should not interfere with the results. For the PMA double-pulse experiment, 100 nM PMA and 1 nM EGF were used. After incubation with the growth factors for the indicated time period, cells were washed three times with phosphate-buffered saline (PBS).

Immunoblotting

Cell lysates were prepared and analyzed as described previously (Birtwistle et al., 2007). For western blot analysis, anti-ERK (p44/42 MAP kinase), anti-phospho-ERK (Thr202/Tyr204), anti-CREB, anti-phospho-CREB (Ser133), anti-MEK1/2, anti-phospho-MEK1/2 (Ser217/221), anti-p90RSK, anti-phospho-p90RSK (Ser380), and anti-α-tubulin antibodies were purchased from Cell Signaling Technology. Anti-Fos antibody was purchased from Santa Cruz Biotechnology. (Santa Cruz, CA). Anti-GAPDH and anti-phospho-Fos (Thr325) antibody were purchased from Abcam (Cambridge, UK). The protein band intensities were quantified with a densitometer (Fuji Film, Japan).

For measurement of ppERK in different cellular compartments, cells were washed twice with ice-cold PBS containing 0.4 mM Na$_3$VO$_4$, scraped into hypotonic lysis buffer (10 mM Tris [pH 7.4], 10 mM NaCl, 3 mM MgCl$_3$, 1 mM EGTA, 1 mM Na$_3$VO$_4$, 10 mM NaF, aprotinin, leupeptin, and PMSF), and incubated on ice for 10 min. The lysate was homogenized with a Dounce homogenizer (40 strokes) and then centrifuged at 8000 g for 5 min. The pellet (nuclear fraction) was washed five times with hypotonic lysis buffer containing 0.1% NP-40 and resuspended in lysis buffer containing 0.5% sodium deoxycholate, 0.1% SDS, and 0.2% NP-40. The soluble fraction was centrifuged at top speed for 5 min and supernatant was considered the cytosolic fraction.

Immunofluorescence

Standard immunofluorescence (Figure 3) was performed as described in the Extended Experimental Procedures. The in situ Proximity Ligation Assay (PLA) with the Duolink kit (OLINK bioscience, Sweden) was used to quantify nuclear ppERK according to the manufacturer's instructions. The Duolink assay has been shown to be much more quantitative and reproducible than standard immunostaining (Fredriksson et al., 2002; Söderberg et al., 2006). These experiments were performed in triplicate, and standard error was calculated based on this sample size of three. The stained cells were analyzed with a TCS-SPE microscope (LAS AF software ver 1.8.2, Leica, Germany). ppERK was detected and quantified with BlobFinder software (OLINK bioscience). DAPI staining was used to identify cell nuclei. Approximately 60 individual cell images were quantified for each time point, and all cells with a whole nucleus within a field of view were quantified. Representative PLA images are given in Figure S3A.

siRNA Transfection

Transfection was performed with the HiperFect Transfection Reagent (QIAGEN) and CombiMAG magnetofection kit (Chemicell GmbH, Germany) according to the manufacturer's instructions. The *dusp 1*, *2*, *4*, and *5* siRNA sequences can be found in the Extended Experimental Procedures. For combination knockdown experiments, 10 nM of each siRNA were transfected, and the results were compared to data from control cells which were transfected with identical concentrations of non-targeting siRNA mixture (40 nM, Control AllStars 1, QIAGEN). We also used a completely independent set of *dusp* siRNAs from Dharmacon for verification of the results (Figure S3D; sequences in the Extended Experimental Procedures). Forty-eight hr after transfection, cells were starved for 16 hr in serum-free DMEM and then stimulated with 10 nM growth hormone for the indicated time periods.

Quantitative RT-PCR

RNA was reverse transcribed into complementary DNA with the PrimeScript RT reagent Kit (TaKaRa, Japan; primer sequences in the Extended Experimental Procedures). All the PCR reactions were done using either SYBR Premix Ex Taq (TaKaRa) or KAPA SYBR Fast kit (KAPA Biosystems, South Africa) in a Thermal Cycler Dice Real Time System TP800 (TaKaRa). qRT-PCR was performed in triplicate for each sample according to the manufacturer's instructions. The standard curve method was used to determine relative quantity of mRNA. All qRT-PCR data were normalized to GAPDH expression.

Model Simulation

We describe the biochemical reactions and connectivity of signaling molecules using ordinary differential equations (ODEs) known as chemical kinetic equations. The ODE models were developed and simulated with MATLAB (Mathworks) and are available from the Biomodels database under the IDs 1004300000 (mechanistic model) and 1003170000 (core model) (http://www.ebi.ac.uk/biomodels/). Detailed descriptions are in the Extended Experimental Procedures.

Model Parameter Estimation

To estimate the unknown model parameters, we minimized the sum of squared differences between the experimental data shown in Figure 1 and the simulated values using the genetic algorithm GLSDC (Kimura and Konagaya, 2003) implemented on 160 CPUs in parallel (for details, see the Extended Experimental Procedures). For the initial model, we obtained 50 good-fitting

parameter sets, and simulation curves represent the mean of 50 independent simulations using these 50 sets (Table S4). Simulation standard deviations were similarly computed. For the refined model, we obtained ten good-fitting parameter sets (Table S4).

Sensitivity and Robustness Analysis

The sensitivity coefficients are defined by

$$C_i^M \equiv d \ln(M)/d \ln(v_i),$$

where M is the signaling metric (time-integrated response or duration—defined in the main text) and v_i is the ith reaction rate. Control coefficients were calculated using finite difference approximations with 0.01% changes in the reaction rates. Calculation validity was tested by verifying that summation laws are obeyed (Kholodenko et al., 1997a), which required use of the MEK empirical model for a non-time dependent model input (see the Extended Experimental Procedures and Figure S2). Robustness is defined as the sum over all inverse, absolute parameter sensitivity coefficients,

$$R = \sum_i |d \ln(p_i)/d \ln(M)|,$$

where p_i is a model parameter.

SUPPLEMENTAL INFORMATION

Supplemental Information includes Extended Experimental Procedures, six figures, and seven tables and can be found with this article online at doi:10.1016/j.cell.2010.03.054.

REFERENCES

Armstrong, S.P., Caunt, C.J., and McArdle, C.A. (2009). Gonadotropin-releasing hormone and protein kinase C signaling to ERK: spatiotemporal regulation of ERK by docking domains and dual-specificity phosphatases. Mol. Endocrinol. *23*, 510–519.

Birtwistle, M.R., Hatakeyama, M., Yumoto, N., Ogunnaike, B.A., Hoek, J.B., and Kholodenko, B.N. (2007). Ligand-dependent responses of the ErbB signaling network: experimental and modeling analyses. Mol. Syst. Biol. *3*, 144.

Brondello, J.M., McKenzie, F.R., Sun, H., Tonks, N.K., and Pouysségur, J. (1995). Constitutive MAP kinase phosphatase (MKP-1) expression blocks G1 specific gene transcription and S-phase entry in fibroblasts. Oncogene *10*, 1895–1904.

Brondello, J.M., Brunet, A., Pouysségur, J., and McKenzie, F.R. (1997). The dual specificity mitogen-activated protein kinase phosphatase-1 and -2 are induced by the p42/p44MAPK cascade. J. Biol. Chem. *272*, 1368–1376.

Brondello, J.M., Pouysségur, J., and McKenzie, F.R. (1999). Reduced MAP kinase phosphatase-1 degradation after p42/p44MAPK-dependent phosphorylation. Science *286*, 2514–2517.

Bruning, J.C., Gillette, J.A., Zhao, Y., Bjorbaeck, C., Kotzka, J., Knebel, B., Avci, H., Hanstein, B., Lingohr, P., Moller, D.E., et al. (2000). Ribosomal subunit kinase-2 is required for growth factor-stimulated transcription of the c-Fos gene. Proc. Natl. Acad. Sci. USA *97*, 2462–2467.

Buchwalter, G., Gross, C., and Wasylyk, B. (2004). Ets ternary complex transcription factors. Gene *324*, 1–14.

Caunt, C.J., Armstrong, S.P., Rivers, C.A., Norman, M.R., and McArdle, C.A. (2008). Spatiotemporal regulation of ERK2 by dual specificity phosphatases. J. Biol. Chem. *283*, 26612–26623.

Chai, J., and Tarnawski, A.S. (2002). Serum response factor: discovery, biochemistry, biological roles and implications for tissue injury healing. J. Physiol. Pharmacol. *53*, 147–157.

Charles, C.H., Abler, A.S., and Lau, L.F. (1992). cDNA sequence of a growth factor-inducible immediate early gene and characterization of its encoded protein. Oncogene *7*, 187–190.

Chen, R.H., Sarnecki, C., and Blenis, J. (1992). Nuclear localization and regulation of erk- and rsk-encoded protein kinases. Mol. Cell. Biol. *12*, 915–927.

Chen, R.H., Abate, C., and Blenis, J. (1993). Phosphorylation of the c-Fos transrepression domain by mitogen-activated protein kinase and 90-kDa ribosomal S6 kinase. Proc. Natl. Acad. Sci. USA *90*, 10952–10956.

Citri, A., and Yarden, Y. (2006). EGF-ERBB signalling: towards the systems level. Nat. Rev. Mol. Cell Biol. *7*, 505–516.

De Cesare, D., Jacquot, S., Hanauer, A., and Sassone-Corsi, P. (1998). Rsk-2 activity is necessary for epidermal growth factor-induced phosphorylation of CREB protein and transcription of c-fos gene. Proc. Natl. Acad. Sci. USA *95*, 12202–12207.

Fredriksson, S., Gullberg, M., Jarvius, J., Olsson, C., Pietras, K., Gústafsdóttir, S.M., Ostman, A., and Landegren, U. (2002). Protein detection using proximity-dependent DNA ligation assays. Nat. Biotechnol. *20*, 473–477.

Gille, H., Kortenjann, M., Thomae, O., Moomaw, C., Slaughter, C., Cobb, M.H., and Shaw, P.E. (1995). ERK phosphorylation potentiates Elk-1-mediated ternary complex formation and transactivation. EMBO J. *14*, 951–962.

Hornberg, J.J., Bruggeman, F.J., Binder, B., Geest, C.R., de Vaate, A.J., Lankelma, J., Heinrich, R., and Westerhoff, H.V. (2005). Principles behind the multifarious control of signal transduction. ERK phosphorylation and kinase/phosphatase control. FEBS J. *272*, 244–258.

Keyse, S.M., and Emslie, E.A. (1992). Oxidative stress and heat shock induce a human gene encoding a protein-tyrosine phosphatase. Nature *359*, 644–647.

Kholodenko, B.N. (2006). Cell-signalling dynamics in time and space. Nat. Rev. Mol. Cell Biol. *7*, 165–176.

Kholodenko, B.N. (2007). Untangling the signalling wires. Nat. Cell Biol. *9*, 247–249.

Kholodenko, B.N., Demin, O.V., and Westerhoff, H.V. (1997a). Control analysis of periodic phenomena in biological systems. J. Phys. Chem. *101*, 2070–2081.

Kholodenko, B.N., Hoek, J.B., Westerhoff, H.V., and Brown, G.C. (1997b). Quantification of information transfer via cellular signal transduction pathways. FEBS Lett. *414*, 430–434.

Kholodenko, B.N., Kiyatkin, A., Bruggeman, F.J., Sontag, E., Westerhoff, H.V., and Hoek, J.B. (2002). Untangling the wires: a strategy to trace functional interactions in signaling and gene networks. Proc. Natl. Acad. Sci. USA *99*, 12841–12846.

Kimura, S., and Konagaya, A. (2003). High Dimensional Function Optimization using a new Genetic Local Search suitable for Parallel Computers. Paper presented at: Int Conf on Systems, Man, and Cybernetics.

Mangan, S., Zaslaver, A., and Alon, U. (2003). The coherent feedforward loop serves as a sign-sensitive delay element in transcription networks. J. Mol. Biol. *334*, 197–204.

Marshall, C.J. (1995). Specificity of receptor tyrosine kinase signaling: transient versus sustained extracellular signal-regulated kinase activation. Cell *80*, 179–185.

Mettetal, J.T., Muzzey, D., Gómez-Uribe, C., and van Oudenaarden, A. (2008). The frequency dependence of osmo-adaptation in Saccharomyces cerevisiae. Science *319*, 482–484.

Murphy, L.O., Smith, S., Chen, R.H., Fingar, D.C., and Blenis, J. (2002). Molecular interpretation of ERK signal duration by immediate early gene products. Nat. Cell Biol. *4*, 556–564.

Murphy, L.O., MacKeigan, J.P., and Blenis, J. (2004). A network of immediate early gene products propagates subtle differences in mitogen-activated protein kinase signal amplitude and duration. Mol. Cell. Biol. *24*, 144–153.

Nagashima, T., Shimodaira, H., Ide, K., Nakakuki, T., Tani, Y., Takahashi, K., Yumoto, N., and Hatakeyama, M. (2007). Quantitative transcriptional control of ErbB receptor signaling undergoes graded to biphasic response for cell differentiation. J. Biol. Chem. *282*, 4045–4056.

Ogunnaike, B.A., and Ray, W.H. (1994). Process Dynamics, Modeling and Control (New York: Oxford University Press).

Pellegrino, M.J., and Stork, P.J. (2006). Sustained activation of extracellular signal-regulated kinase by nerve growth factor regulates c-fos protein stabilization and transactivation in PC12 cells. J. Neurochem. *99*, 1480–1493.

Rivera, V.M., Miranti, C.K., Misra, R.P., Ginty, D.D., Chen, R.H., Blenis, J., and Greenberg, M.E. (1993). A growth factor-induced kinase phosphorylates the serum response factor at a site that regulates its DNA-binding activity. Mol. Cell. Biol. *13*, 6260–6273.

Santos, S.D., Verveer, P.J., and Bastiaens, P.I. (2007). Growth factor-induced MAPK network topology shapes Erk response determining PC-12 cell fate. Nat. Cell Biol. *9*, 324–330.

Sariban, E., Luebbers, R., and Kufe, D. (1988). Transcriptional and posttranscriptional control of c-fos gene expression in human monocytes. Mol. Cell. Biol. *8*, 340–346.

Sauro, H.M., and Kholodenko, B.N. (2004). Quantitative analysis of signaling networks. Prog. Biophys. Mol. Biol. *86*, 5–43.

Schönthal, A., Herrlich, P., Rahmsdorf, H.J., and Ponta, H. (1988). Requirement for fos gene expression in the transcriptional activation of collagenase by other oncogenes and phorbol esters. Cell *54*, 325–334.

Söderberg, O., Gullberg, M., Jarvius, M., Ridderstråle, K., Leuchowius, K.J., Jarvius, J., Wester, K., Hydbring, P., Bahram, F., Larsson, L.G., and Landegren, U. (2006). Direct observation of individual endogenous protein complexes in situ by proximity ligation. Nat. Methods *3*, 995–1000.

Sun, H., Charles, C.H., Lau, L.F., and Tonks, N.K. (1993). MKP-1 (3CH134), an immediate early gene product, is a dual specificity phosphatase that dephosphorylates MAP kinase in vivo. Cell *75*, 487–493.

Superti-Furga, G., Bergers, G., Picard, D., and Busslinger, M. (1991). Hormone-dependent transcriptional regulation and cellular transformation by Fos-steroid receptor fusion proteins. Proc. Natl. Acad. Sci. USA *88*, 5114–5118.

Wang, Y., and Prywes, R. (2000). Activation of the c-fos enhancer by the erk MAP kinase pathway through two sequence elements: the c-fos AP-1 and p62TCF sites. Oncogene *19*, 1379–1385.

Xing, J., Ginty, D.D., and Greenberg, M.E. (1996). Coupling of the RAS-MAPK pathway to gene activation by RSK2, a growth factor-regulated CREB kinase. Science *273*, 959–963.

Zhang, X., Gureasko, J., Shen, K., Cole, P.A., and Kuriyan, J. (2006). An allosteric mechanism for activation of the kinase domain of epidermal growth factor receptor. Cell *125*, 1137–1149.